Sensors and Actuators A 302 (2020) 111768

Contents lists available at ScienceDirect

Sensors and Actuators A: Physical

journal homepage: www.elsevier.com/locate/sna

$LiNbO_3$ Nanocrystals for Tunable Ion Track Electronics and Gas Sensorics

K. Hoppe[a], W. Fahrner[b], A. Petrov[c], D. Fink[d,e,*], V. Hnatowicz[d], J. Vacik[d], D. Bork[f], P. Heitjans[f]

[a] South Westfalia University of Applied Sciences, 58095 Hagen, Germany
[b] Chair of Electronic Devices, Hagen University, 58097 Hagen, Germany
[c] Inst. of Solid State and Semiconductor Physics NAS Belarus, 220072 Minsk, Belarus
[d] Nuclear Physics Institute, ASCR, 25068 Řež, Czech Republic
[e] Departamento de Fisica, Universidad Autónoma Metropolitana-Iztapalapa, PO Box 55-534, 09340 México, D.F, Mexico
[f] Institute of Physical Chemistry and Electrochemistry, Leibniz University Hannover, 30167 Hannover, Germany

ARTICLE INFO

Article history:
Received 8 October 2019
Received in revised form
23 November 2019
Accepted 25 November 2019
Available online 30 November 2019

ABSTRACT

About 20 nm large $LiNbO_3$ nanocrystals are produced by high-energy ball milling, and then suspended in water by surrounding them with amyl acetate ligands. The formed colloids are allowed to penetrate into etched swift heavy ion tracks in an oxide layer on silicon. After appropriate contacting, both a source-drain and a gate voltage are connected to the resulting electronic structure. Depending on the applied external voltages, the current-voltage characteristics shows peculiar properties, ranging from Ohmic-type via forward- or backward-rectifying types up to double-rectifying types, eventually with hysteresis showing up. These structures could become relevant to gas sensorics.

1. Introduction: Advanced electronics exploiting ion tracks in solids

Latent and etched swift heavy ion (SHI) tracks in polymers and silicon dioxide (or other materials with parallel nanopores) have long been thought to become useful substrates in nano- and microelectronics [1]. One idea was to fill etched tracks with conducting material (such as metals or conducting polymers) to form miniaturized parallel wires, and to connect them on their surfaces in a suitable way, to form, e.g., micromagnets, microtransformers or microcapacitors [2,3]. Filling the tracks instead with semiconducting material leads to the formation of miniaturized diodes or transistors [4–6], i.e. to building blocks of "single ion track electronics" (SITE) [7]. The SITE may have various targeted applications. One of the possibilities is, e.g., gas sensors based on nuclear tracks with Li compounds. Both components (etched nuclear tracks and Li solid compounds) have already been used in gas sensorics [8-11], however, a combination of both has never been tested.

Apart from the trivial idea to just scale-down conventional macroscopic electronic elements, one also can exploit the interaction of many parallel conducting tracks with each other to develop novel electronic devices. For example, when putting parallel neighbored nanodiodes on different potentials in a controlled way, their interaction may lead to instabilities that give rise to, e.g., negative differential resistances which are quite useful in electronics, and can be utilized as an effective means for gas sensing [12].

This strategy had been realized by the "TEAMS" concept, with "TEAMS" being an acronym for: "Tunable Electronically Anisotropic Materials on Semiconductors" [13], Fig. 1a. Here, the basic idea was to deposit an electronically anisotropic material (center of Fig. 1b) onto suitable insulating or semiconducting materials (bottom of Fig. 1b) and to combine the directional preference of such materials with the electronic properties of "classical" semiconductors such as silicon. In order to allow each point on the surface of the anisotropic layer to have access to charge carriers in a controlled way, usually some high-resistivity material is added on that layer (top of Fig. 1b). For the anisotropic central layer, either naturally-grown electronically anisotropic materials (such as SnO_2, C_{60}, etc.) can be used. Alternatively, also isotropically conducting semiconductor materials (such as Ag carbamate [14]) can be deposited on a substrate and subsequently be irradiated with swift heavy ions (SHI). In the latter case, it is the highly localized transfer of high electronic energy to the target material along the trails of highly energetic heavy ions that changes the target materials electronic properties within a tiny zone of a few nm diameter (the so-called track core) via a chain of

* Corresponding author at: Nuclear Physics Institute, ASCR, 25068 Řež, Czech Republic.
E-mail address: fink@xanum.uam.mx (D. Fink).

https://doi.org/10.1016/j.sna.2019.111768
0924-4247/

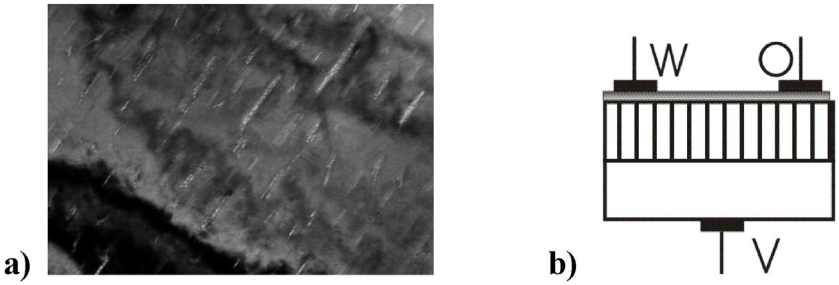

Fig. 1. a) This TEM micrograph explains the basic idea to impose anisotropy on any material by means of energetic ion impact. The parallel ion tracks, if made (semi)conducting by insertion of any suitable (semi)conducting material (eventually after etching), make the host material electrically anisotropically (semi)conducing in the SHI's impact direction. Shown here for illustration is a historic TEM picture of 29.6 MeV Helium ion tracks in MoO_3 (courtesy by L.T.Chadderton 1998). b) Principle sketch of a TEAMS structure. Top (grey): highly resistive contact layer (if necessary), center (with stripes, to symbolize the (semi)conducting tracks): anisotropic layer, bottom (plain white): semiconducting substrate. The TEAMS device is connected by the top contacts ***w*** and ***o*** and a bottom contact ***v*** (they are occasionally denoted as "source", "gate" and" drain" in analogy to the familiar transistors, but must not be confused with them).

complex processes [15]. The radiation-modified zones are straight and very long (up to ~ 100 μm) but very narrow (typically a few nm in radius) regions, the so-called "ion tracks" or "latent tracks". Depending on the type of irradiated material, its electronic parameters such as the conductivity, mobility, relative permittivity etc. can either be increased or decreased.

If for some reason, isotropic insulating materials (such as SiO_2, photoresist, polyimide, etc.) are preferred instead as central layers, which usually do not suffer any major conductivity changes along their latent tracks by the SHI irradiation, one can dissolve (etch) these latent tracks with suitable reactive agents so that parallel extended narrow pores (etched tracks) are formed, into which thereafter suitable (semi)conducting materials are inserted. Thus, the conductivity along the track direction is enhanced greatly whereas ~zero conductivity remains along directions perpendicular to the tracks, i.e. these layers acquire their highest possible electronic anisotropy. These special TEAMS structures have become known as: "TEMPOSstructures, which stands for: "Tuneable Electronic Material in Pores in Oxide on Semiconductors" [15].

For their application in electronic circuits, TEAMS structures (including their TEMPOS subgroup) are usually connected with two electrodes ***w*** and ***o*** (occasionally being denoted, due to their first-glance analogy to conventional transistors, also as the "source" and "gate" electrodes – though TEAMS structures are by no means transistors!) on different places of the anisotropic top layer and one electrode *v* ("drain") on the semiconducting substrate, Fig. 1b. The current/voltage characteristics of these structures are determined by the type of both the anisotropic material and the substrate, the interaction of the top layer with the ambient (if the material has sensor properties), the device's size and geometrical arrangement (which determines the ratio of the resistances and capacities between the contacts), and the track-to-track interactions. Depending on the above-listed properties, the current/voltage characteristics usually resemble those ones of tunable resistors, capacitors, diodes, transistors or sensors [13].

Hitherto, TEAMS structures with latent SHI tracks were produced which exploited fullerite layers (where the tracks are sp2 enriched zones) [16], Ag carbamate layers (where the latent tracks are essentially silver sulfide-type precipitates) [17], and polysilane layers (where the latent tracks consist of SiC wires) [18]. Also, TEAMS structures with etched tracks in SiO_2 layers - i.e., TEMPOS structures – were prepared, where the etched tracks were filled with fullerite [19], phthalocyanine [20], Ag nanoparticles [15], Au nanoparticles [21], TiO_2 colloids (i.e., TiO_2 nanoclusters surrounded by a shell of organic ligands) [22], PbSe and CdTe colloids [23], PEO/CdS composite colloids (by intermixing them with different host materials) [24], and finally Au/Teflon composite colloides [25]. TEMPOS structures with tracks filled with ion or mixed conductors showed the sensing to ammonia gas [9].

In this work we report the first results which have been obtained with $LiNbO_3$ colloidal nanoparticles inserted into etched tracks of TEMPOS structures. $LiNbO_3$ had been studied already by some of us before, by Nuclear Magnetic Resonance (NMR) of the ^7Li and ^8Li isotopes [26–31,33], impedance spectroscopy [32–33], extended X-ray absorption fine structure spectroscopy [33], secondary ion mass spectroscopy [34,35] and neutron reflectometry [36]. Due to the well-known attractive optoelectronic, electrooptic, piezoelectronic, and accustoelectronic properties of $LiNbO_3$, devices such as directional couplers, switches, ring resonators [37], modulators, deflectors, and RF spectrum analyzers have been realized with this material already since nearly 5 decades, exploiting the possibility to construct, e.g., optical waveguides circuits [38] of this material. Of special interest are structures where $LiNbO_3$ undergoes intimate contact with SiO_2 and Si [37,38]. Having this in mind, we thought it worthwhile to obtain first information about the electronic behavior of TEMPOS structures with inserted lithium niobate, to study at a later stage also their optoelectronic and gas-sensing behavior.

2. Experimental: Production of TEMPOS structures with $LiNbO_3$ nanocrystalline colloides

2.1. Preparation of the substrates with etched tracks

Self-prepared Si/SiO_2 bilayer structures, and for comparison also "Melinex" foils (= polyethylene terephthalate, PET of Russian origin) were irradiated by swift heavy ions at the ISL accelerator of the former HMI Berlin and the JNRI accelerator in Dubna, respectively, and then etched with the appropriate agents. The parameters used for these experiments are compiled in Table 1. The ion track etching was performed under different conditions according to well-known

Table 1
Production parameters of the etched tracks to be filled with the $LiNbO_3$ nanocrystals.

Substrate material	SiO_2 on Si (bilayer structure)	PET (polymer foil)
Thickness of track-bearing layer [μm]	~0.1 to 0.2	10
Swift heavy ion: type,	$^{191}Au^{26+}$	$^{84}Kr^{14+}$
Energy [MeV]	350 MeV	210 MeV
Fluence [cm^{-2}]	1×10^8	2×10^8
Etchant	HF, 4%	NaOH, 5 mole/l
Etching temperature	R.T.	80. . .90 °C
Etching time	several minutes	few minutes
Etched track radii [nm]	~150-180 ~200-230	~50 to 200

recipes [4], to produce etch tracks of different sizes and internal geometries such as cylindrical, conical and funnel-shaped pores.

2.2. $LiNbO_3$ nanoparticle preparation and characterization

$LiNbO_3$ nanoparticles can be produced by either the sol/gel technique or via high-energy ball milling [26–28]. In this work, we used the latter approach. For this sake, commercially available crystalline $LiNbO_3$ powder was used as starting material. Its crystallites have sizes of about 1.5 μm according to transmission electron microscopy (TEM) [27], and of 0.4 to 0.53 μm according to X ray diffraction (XRD) measurements. The difference in size may be explained by the agglomeration of the smaller-sized crystals to the larger particles observed by TEM.

After 128 hours of milling these crystals in a high-energy ball mill (SPEX 8000), particles of typically 20 nm size are obtained [39]. These nanoparticles use to stick strongly together, forming aggregates of micrometer size. Therefore, if poured into water and stirred, the clustered nanometric material sediments rather quickly. Nevertheless XRD analysis of such micrometer-sized aggregates reveals grain sizes of some (45 ± 10) nm, indicating that these large aggregates really consist of much smaller structural units. This analysis is based on two different approaches, the one using the Debye-Scherrer formula [40], and another one from Williamson and Hall [41]. Both techniques make use of the fact that X-ray diffraction signals become broader with decreasing crystal sizes. The first approach restricts to spherical particles and neglects the eventual lattice strain in the material. Here, the exact line shape is not known and the line width is not corrected. For contrast, the Williams-Hall plots imply Lorentzian line shapes and take into account micro-tensions. In the first case, the linear particle size b is derived from the measured line broadening full width half maximum (FWHM) and the Bragg angle ξ of the scattered X rays with the wavelength λ, to be:

$$b = 0.9\lambda/(\mathrm{FWHM}\cos(\xi)) \quad (1)$$

In the second case, a plot of FWHM cos(ξ) vs. sin(ξ) (or of δs vs. s^2), the so-called Williamson-Hall plot, is used to separate the particle size term from the elastic strain field part. Here, δs describes the broadening of the X ray diffraction peaks, which is measured in units of $s = 2\sin(\xi)/\lambda$. The evaluation of several measured diffraction peaks shows a very small influence of the elastic strain term onto these plots. Both the Scherrer evaluation and the Williams-Hall plot result in comparable particle radii.

2.3. Preparation of colloidal $LiNbO_3$ solution

The ball-milled $LiNbO_3$ agglomerates had to be reduced to their nano-components first, before using them appropriately. This has been achieved by treating them in amyl acetate solution in an ultrasonic bath for about one day at around 35^0 C. Under these conditions part of the clusters break apart, and the released nanocrystals are stabilized in the liquid by the addition of the organic ligands. During this process, not all the material is colloidally dissolved. The remaining larger $LiNbO_3$ clusters are sedimented by centrifugation. The colloidal $LiNbO_3$ suspension is found to be stable within more than ∼ 5 years, without nearly any further sedimentation. It has an orange color, in contrast to the white $LiNbO_3$ and the colorless organic solvent. This colloidal suspension is relatively viscous and hardly solidifies under ambient conditions. Even after annealing for 2 days at ∼ 150 °C, or 230 °C for 1 hour in ambient air, or after vacuum drying, it maintains a somewhat tar-like consistency.

TEM revealed that the sedimented fraction looked quite similar to the original ball-milled material. The suspended colloidal particles (see Fig. 6.6b on p. 241 of Ref. [4]) have diameters of some 30 to 50 nm, roughly in accordance with XRD measurements (see below) which yield average particle sizes of about (27 ± 7) nm. It is remarkable that they have a pronouncedly spherical appearance which points at some surface dissolution by the organic liquid. Besides these particles, another fraction of spherical clusters of some 200 nm diameter showed up in the TEM pictures which was considered as an artifact of the TEM sample preparation due to clustering of some of the nanoparticles during sample drying.

Table 2
Diameters of $LiNbO_3$ nanocrystallites, as determined by TEM and XRD analysis under various conditions.

Procedure	TEM results [nm]	XRD results [nm]
Commercially obtained raw material	(1500 ± 300)	400 to 530
Smallest obtained particles after ball milling, dry	(20 ± 10) -	- (45 ± 10)
Sedimented fraction after suspension in water only		
Colloide $LiNbO_3$ suspension	30 to 50	(27 ± 7)
Additional cluster nanoparticle fraction in TEM micrographs	(200 ± 20)	-

The XRD patterns could not be obtained straightforwardly. Only after background subtraction of the corresponding XRD raw spectra, faint but clearly visible XRD peaks showed up (see, e.g. Fig. 6.6b on p. 241 of Ref. [4]) which indicate that the $LiNbO_3$ particles were not simply dissolved in the solution but still remain in crystalline shape, hence that one deals here with a suspension of colloidal nanocrystals. Consequently Li^+ ions are hardly found in the liquid - their abundance, if any, is less than $5x10^{-3}$ cm^{-3} atomic fraction, as could be verified by the test reaction: $Li^+ + F^- \rightarrow LiF\downarrow$ producing insoluble - hence easily detectable (via Neutron Depth Profiling, NDP [42]) - LiF. In fact, this expands the earlier knowledge that $LiNbO_3$ is rather insoluble in water, also to the nanometer scale. Broad peaks in the XRD spectra of the colloidal suspension clearly revealed that we deal here with *nano* crystalline $LiNbO_3$. The sizes of all $LiNbO_3$ particles as determined by TEM and XRD after the various steps of preparation are compared in Table 2.

Elemental analysis by EDAX, XRD, and NDP reveals that all these particles consist indeed of $LiNbO_3$. For this sake droplets of the suspensions were dried on TEM grids or clean Si wafers, respectively, by heating up to 230^0 C for 1 h, and then probed. Indeed, in the EDAX spectra a pronounced Nb-K-line showed up, and from the NDP spectra pronounced Li depth profiles could be derived.

2.4. $LiNbO_3$ nanocrystal penetration into etched tracks

The penetration of the $LiNbO_3$ colloides into the etched tracks can be nicely followed by NDP. Here, the ^6Li component serves as probe, for which the depth distributions can be recorded with high accuracy and sensitivity, and up to great depths, by exploiting the non-destructive NDP technique [42]. In this approach one localizes the Li component via the nuclear reaction $^6Li(n,\alpha)^3H$ with thermal or cold neutrons. The energy loss spectra of both the alphas and tritons can be evaluated, the α spectrum giving a detailed view of the surface-near distribution (with typically 30 nm depth resolution and within the first 3-5 μm), and the ^3H spectrum giving an overview of up to some 50 μm depth, however with about 5 times worse depth resolution. In our case we restrict to the triton distributions, as the depth interval of interest is in the order of 10 μm.

For the conversion of the measured energy spectra to depth distributions, we use the triton stopping power in the materials hosting the etched tracks (in our case: polyethylene terephthalate (PET, "mylar") as test material and SiO_2 of the TEMPOS struc-

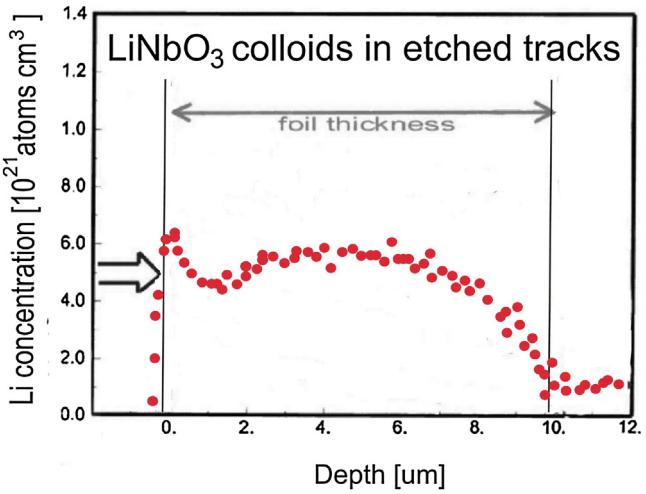

Fig. 2. Typical depth profile of $LiNbO_3$ nanocrystals in cylindrical etched tracks in PET foils, snapshot during slow penetration into horizontally arranged foil (i.e., perpendicularly arranged tracks) under the influence of gravity. The left arrow indicates the direction of $LiNbO_3$ penetration; the depth scale runs from the upper to the lower foil surface. The graph is a combination *of two NDP measurements from both foil sides.*

tures), as calculated by the ZBL theory [43]. This is possible, as the embedded $LiNbO_3$ crystallites contribute negligibly to the stopping powers, due to their overall quite small abundances. (Instead of using the NDP technique, one could have RBS to probe that material, via detection of the Nb depth distribution. However, though RBS exhibits a somewhat better depth resolution than NDP, it has a lower detection sensitivity, and hence might fail for the comparatively low nanocrystal concentrations with which we deal here.)

Our first attempts to pour the large as-prepared ball-milled $LiNbO_3$ grains in water suspension directly into ion tracks of 50 to 200 nm radius (either in polymeric test foils, or in TEMPOS base structures) failed, as all grains became stuck at the track entrance. This conclusion followed clearly from the corresponding Li depth distributions which were taken by NDP (not shown here), where only Li surface peaks showed up. (In other words, the etched tracks acted here as filters for the particles - a destination for which they are actually used most frequently in technology.)

For contrast, the $LiNbO_3$ suspension penetrated into the tracks successfully, for whatever etched track shape (as examples, see Fig. 2 of this paper, and Fig. 3.18 on p. 123 in Ref. [4]). In all cases, the NDP Li depth distributions C(x) reflected the pore shapes nicely according to: $C(x) = C_0\ \pi\ r(x)^2$, with r(x) being the ion track radius at a given depth x, and C_0 being the volume concentration of our orange $LiNbO_3$ suspension (about 10%). Due to the relatively large viscosity of the penetrating colloidal solution, the penetration proceeded slowly, until after typically a few min exposure time, the measured concentration distributions assumed a stationary shape.

The measured overall Li concentration in the porous test foils (in the order of 1%) can be compared with the overall available free track volume in these microporous foils (in the order of 10%) to estimate the degree of filling of the tracks. Consistently with the volume concentration C_0 of the $LiNbO_3$ nanoparticles in the used suspension, it turns out that the nanoparticles fill up only around 10% of the total ion track volume. SEM observation showed that after drying the samples, the $LiNbO_3$ colloides preferentially cover the track walls so that some kind of $LiNbO_3$ nanotubules emerge, however, unfortunately they are still with rather irregular wall thicknesses. Also ion transmission spectrometry (ITS) experiments indicate that these $LiNbO_3$ nanostructures are more or less hollow in their interior.

These results put $LiNbO_3$ into the list of earlier experiments on incorporation of nanosized ceramic matter (such as TiO_2, ZnO, WO_3, and SiO_2 [4]) into nanopores. However, in all the latter cases, the incorporation had followed the sol-gel route, i.e. corresponding sols had been filled into polymeric (or ceramic) porous membranes, and then transformed to gel (aggregated sol particles) on the pore walls. Longer immersion times of the tracks in the gel may lead to their complete filling, i.e. to fibrille formation [4].

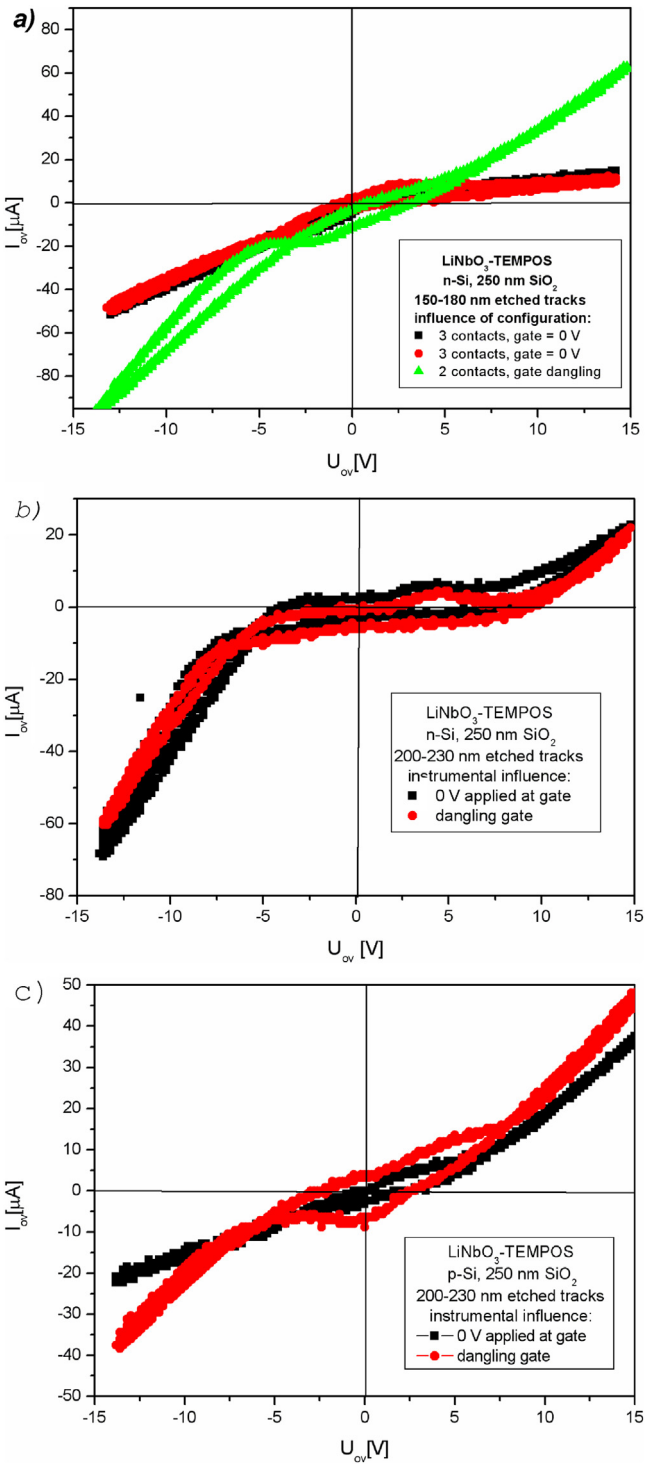

Fig. 3. Current/voltage characteristics of $LiNbO_3$-TEMPOS structures, with dangling gate (contact ***o***) or gate at ground potential, for etched track radii of a) 150-180 or b, c) 200-230 nm, on a,b) n-Si and c) p-Si. a) When exchanging the two top electrodes ***w*** and ***o***, the characteristics (black rectangles and red circles, respectively) remain virtually the same, as the device is constructed symmetrically.

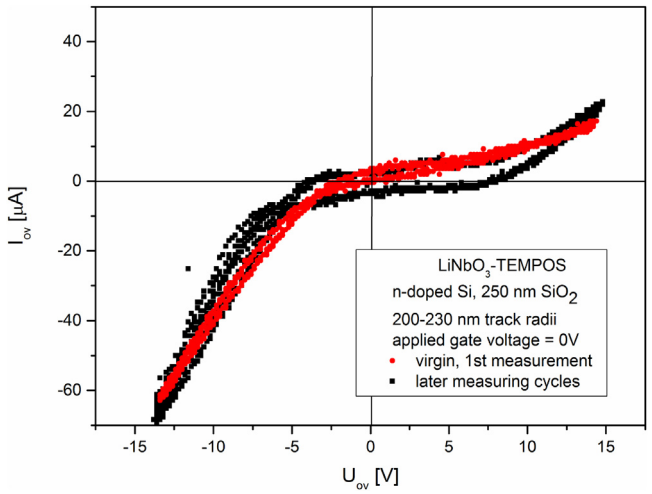

Fig. 4. After the first application of voltage to a virgin sample, there is some slight but permanent change in the current/voltage characteristics of $LiNbO_3$-TEMPOS structures, with gate on ground potential.

After having inserted the orange $LiNbO_3$ colloidal suspension into the etched tracks of the raw SiO_2/Si TEMPOS substrates, the superficial colloides are wiped off with a soft cloth and the structure is dried at elevated temperature (~60 °C). It is seen in Fig. 2 that, after such a procedure, some slight surface Li enrichment remains, which points at some residual $LiNbO_3$ colloides being irregularly distributed on the TEMPOS structure's surface. Measurements of the non-zero conductivity of the $LiNbO_3$-TEMPOS surface indicate that these colloides form the desired conducting top film on the anisotropic layer of Fig. 1b. The surface conductivity is attributed to either charge carrier hopping between the colloides and/or to ionic migration (due to residual water attached to the colloides). If, for some reason, that surface conductivity would prove to be insufficient for major currents to flow, one could additionally deposit onto the TEMPOS surfaces, e.g., some dispersed Au or Ag nanoparticles [15,21] – but this was not necessary here. The required electric contacts were made by depositing small (~ 10 mm^2 contact area) droplets of Ag paste onto the sample surface.

3. Results: First electronic tests with $LiNbO_3$-TEMPOS structures

The successful penetration of the $LiNbO_3$ colloidal solution into etched tracks in SiO_2 on Si could also be reconfirmed in a completely different way, namely by measuring the ion track conductivity. Whereas the latter is virtually zero without the presence of $LiNbO_3$, it rises to pronounced non-zero values after the incorporation and drying of the colloidal niobate solution. Probably the conductivity is of ionic type, stemming from residual water molecules attached to the ligands around the niobate nanocrystals. Several tests were performed which are depicted in Figs. 3–5.

a) Exchanging both "source" and "gate" electrodes ***w*** and ***o*** in some measurement (i.e., examining the ***o***-*v* circuit instead of the ***w***-***v*** one) does not modify the measured current/voltage characteristics, Fig. 3a. This is a consequence of selecting identical geometries for both top electrodes ***o*** and ***w***; any deviation from this geometry results indeed in different characteristics (not shown here).
b) The characteristics of the ***w***-***o*** connection on the $LiNbO_3$-TEMPOS surface (with "drain" electrode *v* floating) is purely Ohmic (not shown). It is thought to stem from the residual homogeneously deposited $LiNbO_3$ colloids on the sample surface, which form the desired conducting top film on the anisotropic layer of Fig. 1b.
c) Fig. 3a also illustrates the difference between devices connected with three contacts (two (***w,o***) on top, one (*v*) on bottom) and with only two contacts (one (***w***) on top, one (*v*) at the bottom). The latter configuration was realized by letting the third (gate) electrode ***o*** dangling. Also this result is obvious: when putting two points on the surface of a TEAMS structure onto two different non-zero potentials, any other point on the surface will assume a well-defined (usually non-zero) potential resulting from the overall equilibrated surface potential distribution. When setting this point intentionally to zero potential, the overall surface potential distribution will be disturbed and some current will flow, i.e. the overall current/voltage (I/V) characteristics will change.
d) Interestingly, for the sample used in Fig. 3b there was found a slight peak at ~ +4.1 V for the upper branches, independent of measuring with or without floating gate. It points at a transient increase in sample capacity for decreasing applied voltage, due to yet unknown reason. Also the inflation of the characteristics of many other cases shown here points at yet poorly understood transient capacitive effects in the sample.
e) In order to understand the influence of the track radius (which primarily influences the track conductivity of course via the amount of incorporated material), we performed all experiments for two different groups of samples: on the one hand, for etched tracks with 150 to 180 nm radius, and on the other hand, for etched tracks with 200 to 230 nm radius (as determined by SEM imaging), both embedded within 250 nm thick SiO_2 layers on either n-Si or p-Si substrates. Whereas for small ion track radii, a pronounced difference shows up between dangling gate and gate fixed at ground potential (Fig. 3a), this difference vanishes for thicker etched tracks, as well in the case of n-Si (Fig. 3b) and p-Si (Fig. 3c) substrates. It is not yet understood why different track radii change the characteristics in the observed way.
f) Comparison between Figs. 3b) and c) shows that the Si doping polarity influences the shape of the characteristics to some extent as samples with n-Si look more double diode-like and the ones with p-Si are more Ohmic-like. In all cases, a small but pronounced central hysteresis can be seen which could eventually be attributed to the water bond in the organic ligand layer of the nanocrystals.
g) Fig. 4 shows that virgin samples require some "formation" till their current/voltage characteristics becomes reproducible. During the very first application of voltage to a virgin sample (red circles), the characteristics exhibit a slightly worse double-diode characteristics and less capacitive effects than later (black squares).
h) Finally, Fig. 5a-d shows the gating voltage dependence (at electrode ***o***) for all combinations of substrate polarity and track radius. A strong dependence on these parameters is recognized. One sees that as well the Si doping as the amount of embedded $LiNbO_3$ have pronounced influences on the device's behavior. The equidistant increase of the applied gate voltage does not necessarily signify a smooth alteration of the characteristics; eventually strong alterations in the curve shapes may show up.

Summarizing, all measured characteristics are combinations of diode-type and Ohmic-type features, plus hysteresis effects. Up to now, no case of negative differential resistances was ever found for this system. The prepared structures were stable for at least half a decade; further aging essentially affected the Ag paste contacts which eventually corroded or even detached. To ensure future

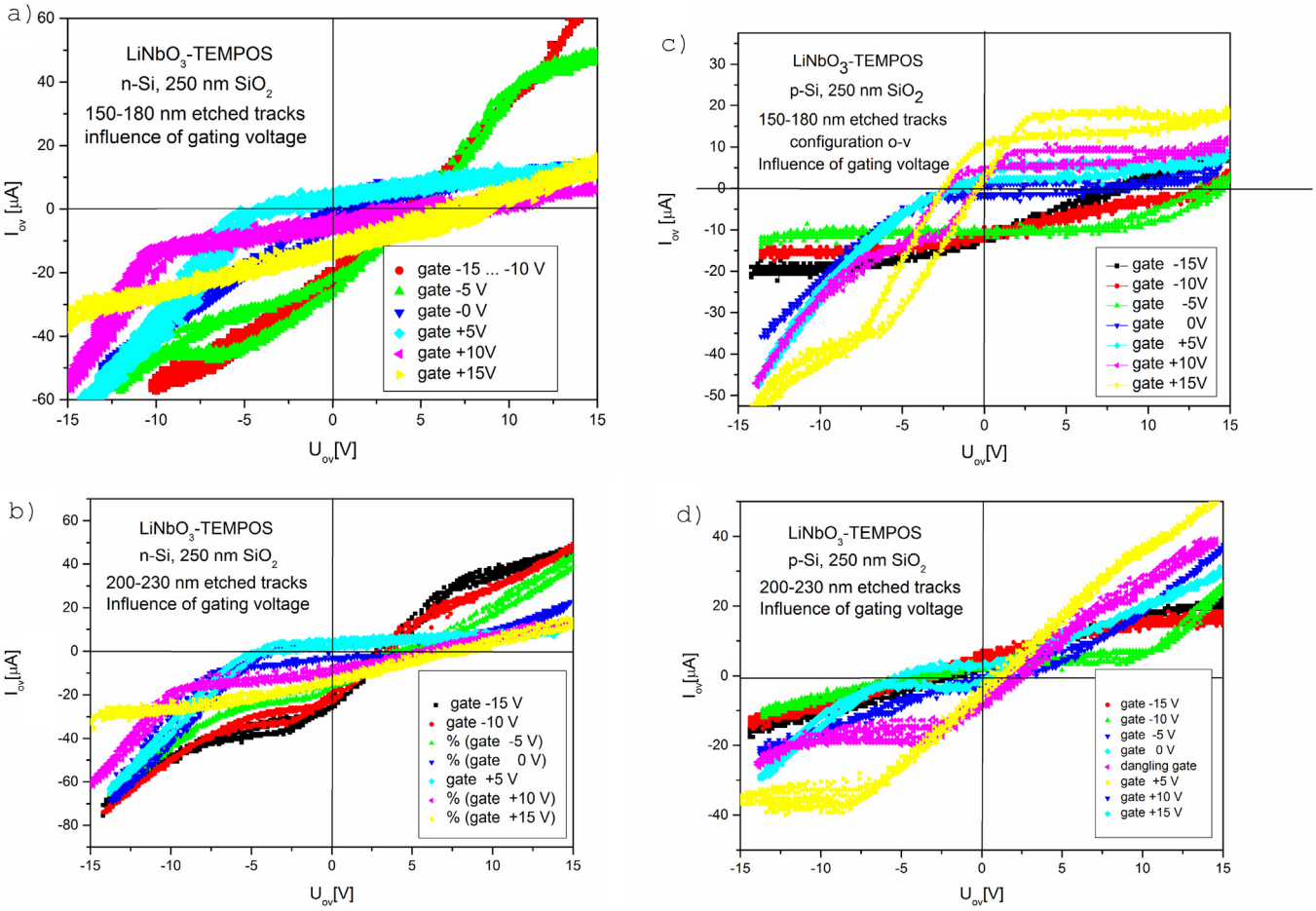

Fig. 5. Dependence of current/voltage characteristics of $LiNbO_3$-TEMPOS structures on the gating voltage (applied at electrode ***o***), for a) n-Si and etched track radii of 150-180 nm, b) n-Si and etched track radii of 200-230 nm, c) p-Si and etched track radii of 150-180 nm, d) p-Si and etched track radii of 200-230 nm.

longer useful device life, the contacts should be replaced by evaporated Au contacts.

4. Conclusions

It is shown that it is possible to accommodate $LiNbO_3$ nanocrystals within cylindrical volumes of 10 µm length and submicrometric radii in a suitable organic (such as thin polymer foils) or inorganic matrix (such as TEMPOS structures), by casting colloidal suspensions of these nanocrystals into pores of preselected shapes inside these materials. The corresponding suspensions are formed by surrounding ball-milled $LiNbO_3$ nanocrystals with suitable hydrophilic ligands such as amyl acetate in aqueous solution. The presently obtained filling factor of these tracks is in the order of 10%, which signifies that the inserted $LiNbO_3$ forms hollow nanowires within the etched tracks. Such nanotubules, in contact with a silicon substrate and suitable surface contacts, exhibit the expected electronic properties, which are combinations of diode-like, Ohmic, and hysteresis effects.

It is at present difficult to draw further conclusions, as a general theory on TEAMS structures is still largely missing. However, as the approach to incorporate lithium niobite into TEMPOS structures was successful, it will now be worthwhile to find out in how far these structures might become useful for applications in gas sensorics, optoelectronics, and others. Especially the hollow geometry of the $LiNbO_3$-clad etched tracks is useful for gas sensing, as it will enable gas to penetrate rapidly. Corresponding tests are planned, especially for ammonia sensing.

- There does not exist any conflict of interest in that paper.
- We, the authors of that paper, declare that we have done that work ourselves, and that we all agree with publishing it as it is.

Acknowledgements

A part of this work (yet unpublished) was performed more than a decade ago at the former Hahn-Meitner-Institute (HMI) Berlin. We are specially obliged to Mrs. Bloeck and to Dr. Giersick, both from former HMI Berlin, for performing the TEM imaging. Also thanks to Dr. P. Apel from JINR Dubna for providing us with the nanoporous PET foils used here, and to the crew of the former swift heavy ion accelerator ISL at HMI Berlin, for enabling the irradiation of the Si/SiO_2 structures. Finally, we are obliged to Prof. L.T.Chadderton (formerly: ANU Canberra; now deceased) for leaving us the TEM micrograph for illustration of the technique of anisotropization of materials by energetic ion impact. D.F. thanks the Universidad Autónoma Metropolitana, Cuajimalpa, México City for his former invitation as guest researcher in the frame of the Cathedra "Alonso Fernandez", and J.V. the Grant Agency of the Czech Republic (No. 19-02804S) regarding the possible application of these novel nanostructures as gas sensors. P. H. is grateful to the Deutsche Forschungsgemeinschaft (DFG) for financial support in

the frame of the former SFB 173 with respect to high-energy ball milling.

References

[1] R. Spohr, in: K. Bethge (Ed.), Ion Tracks and Microtechnology; Principles and Applications, Vieweg, Braunschweig, 1990.
[2] A. Petrov, Production of micro- and nanoelectrotechnic devices based on ion tracks in insulators, PhD. Thesis, Fernuniversität Hagen, Germany, 2004.
[3] Y.N. Shunin, A.E. Kiv (Eds.), Nanodevices and Nanomaterials for Ecological Security, NATO Science for Peace and Security, Series B: Physics and Biophysics, Springer Science, Dordrecht, The Netherlands, 2012.
[4] Transport Processes in Ion Irradiated Polymers and Applications, in: D. Fink (Ed.), Springer Series in Materials Science, vol. 65, Springer, Berlin/Heidelberg/New York, 2004.
[5] D. Fink, P.S. Alegaonkar, A.V. Petrov, A.V. Berdinsky, V. Rao, M. Müller, K.K. Dwivedi, L.T. Chadderton, The emergence of new ion track applications, Radiat. Meas. 36 (2003) 605–609.
[6] D. Fink, P.S. Alegaonkar, A.V. Petrov, M. Wilhelm, P. Szimkowiak, M. Behar, D. Sinha, W.R. Fahrner, K. Hoppe, L.T. Chadderton, High Energy Ion Beam Irradiation of Polymers for Electronic Applications, Nucl. Instr. Meth. B 236 (2005) 11–20.
[7] D. Fink, R. Klett, Latent Ion Tracks in Polymers for Future Use in Nanoelectronics: An Overview of the Present State-of-the-Art, Braz. J. Phys. 25 (1995) 54–75.
[8] A. Sharma, M. Sharma, Ion Tracks-Based Sensors, International Journal of Research in Engineering & Applied Sciences 2 (10) (2012) 1–7.
[9] M. Saroch, S. Srivastava, D. Fink, A. Chandra, Room Temperature Ammonia Gas Sensing Using Mixed Conductor based TEMPOS Structures, Sensors (Basel) 8 (10) (2008) 6355–6370.
[11] W.S. Noh, L. Satyanarayana, J.S. Park, Potentiometric CO Sensor Using Li Ion Conducting Li PO Thin Film Electrolyte, Sensors (Basel) 5 (11) (2005) 465–472.
[12] C. Lao, Yi Li, C.P. Wong, Z.L. Wang, Enhancing the Electrical and Optoelectronic Performance of Nanobelt Devices by Molecular Surface Functionalization, Nano Letters 7 (5) (2007) 1323–1328.
[13] D. Fink, Novel ion track-based electronic structures - an overview, ISL-Information (May) (2005) 2–5 (published by: Hahn-Meitner-Institute Berlin).
[14] A. Kiv, D. Fink, G. Munoz, H.J. Vacik, V. Hnatowicz, Negative Differential Resistance of Aged Organometal/Si Bilayer Structures, Rad. Eff. Def. Solids 174 (2019) 92–110.
[15] D. Fink, A. Petrov, K. Hoppe, W.R. Fahrner, R.M. Papaleo, A. Berdinsky, A. Chandra, A. Chemseddine, A. Zrineh, A. Biswas, L.T. Chadderton, Etched ion tracks in silicon oxide and silicon oxynitride as charge injection or extraction channels for novel electronic structures, Nucl. Instr. Meth. B218 (2004) 355–361.
[16] A.S. Berdinsky, D. Fink, J.B. Yoo, H.G. Chun, L.T. Chadderton, A. Petrov, Conducting properties of planar irradiated and pristine silicon-fullerite-metal structures, Appl. Phys. A, Mat. Sci. & Processing 80 (2005) 1711–1715.
[17] D. Fink, D. Sinha, J. Opitz-Coutureau, A. Petrov, S.E. Demyanov, V.E. Borisenko, W.R. Fahrner, K. Hoppe, A.K. Fedotov, L.T. Chadderton, A.S. Berdinsky, Nanotechnology with Ion Track-Tailored Media, in: S.V. Gaponenko, V.S. Gurin (Eds.), Physics, Chemistry and Application of Nano-Structures, World Scientific Publ., 2005, pp. 474–481.
[18] D. Fink, A. Chandra, W.R. Fahrner, K. Hoppe, R.M. Papaleo, L.T. Chadderton, Tunable Electronically anisotropic materials with Ion-irradiated polysilanes on Semiconductor, Appl. Physics A86 (2007) 469–476.
[19] D. Fink, A. Petrov, K. Hoppe, W.R. Fahrner, Characterization of ẗEMPOS: A new Tunable Electronic Material with Pores in Oxide on Silicon, in: Lu-Min Wang, R. Fromknecht, L. Snead, D.F. Downey, H. Takahasi (Eds.), Proc. MRS Fall Meeting, Boston, Dec. 1-5, vol. 792, 2003 (eds.); R 7.9.
[20] A.V. Petrov, D. Fink, W.R. Fahrner, K. Hoppe, S.E. Demyanov, A.K. Fedotov, A. Zrineh, in: Sensors On The Base Of Zn – Phthalocyanine Tempos Structures, presented at the Int. Conf. on Swift Heavy Ions in Matter, Aschaffenburg, Germany, 2005, unpublished.
[21] D. Sinha, A. Petrov, D. Fink, W.R. Fahrner, K. Hoppe, A. Chandra, TEMPOS structures with Gold Nanoclusters, Rad. Eff. Def. Sol. 159 (2004) 517–533.
[22] D. Fink, A. Petrov, J. Rojas-Chapana, H. Tributsch, D. Friedrich, U. Küppers, M. Wilhelm, P. Yu, A. Zrineh Apel, The Ärtificial Ostrich EggshellP̈roject: sterilizing polymer foils for food industry and medicine, Proc. 8th Intl. Conf. on Condensed Matter and Statistical Physics, Marrakech-Morocco, September 21-24/2004 (2019).
[23] D.K. Ivanou, E.A. Streltsov, A.K. Fedotov, A.V. Mazanik, D. Fink, A. Petrov, Electrochemical Deposition of PbSe and CdTe Nanoparticles onto P-Si (100) Wafers and into Nanopores in Sio2SiO2|Si (100) Structure, Thin Solid Films 490 (2005) 154–160.
[24] A. Chandra, M. Saroch, M. Kumar, A. Petrov, D. Fink, CdS/PEO Semiconductor Dispersed Polymer Electrolytes: Production and Applications, Presented at the Intl. Conf. on Solid State Ionics, Baden-Baden, Germany (2005), July 2005; unpublished.
[25] D. Fink, A. Biswas, A. Petrov, W.R. Fahrner, K. Hoppe, A. Demyanov, F. Faupel, Polymer/Metal Nanocomposites and Ion Tracks, Presented at the Intl. Workshop on Polymer/Metal Nanocomposites, Kiel, Germany (2003), Sept. 22-23, 2003; (unpublished).
[26] D. Bork, PhD. Thesis, University of Hannover, 1997.
[27] D. Bork, P. Heitjans, NMR Relaxation Study of Ion Dynamics in Nanocrystalline and Polycrystalline $LiNbO_3$, J. Phys. Chem. B 102 (1998) 7303–7306.
[28] D. Bork, P. Heitjans, NMR Investigations on Ion Dynamics and Structure in Nanocrystalline and Polycrystalline $LiNbO_3$, J. Phys. Chem. B 105 (2001) 9162–9170.
[29] M. Wilkening, D. Bork, S. Indris, P. Heitjans, Diffusion in Amorphous $LiNbO_3$ Studied by ^{7}Li-NMR – Comparison with the Nano- and Microcrystalline Material, Phys. Chem. Chem. Phys. 4 (2002) 3246–3251.
[30] M. Wilkening, P. Heitjans, New Prospects in Studying Li Diffusion – Two-Time Stimulated Echo NMR of Spin-3/2 Nuclei, Solid State Ionics 177 (2006) 3031–3036.
[31] P. Heitjans, A. Schirmer, S. Indris, NMR and β-NMR Studies of Diffusion in Interface-Dominated and Disordered Solids, in: P. Heitjans, J. Kärger (Eds.), Diffusion in Condensed Matter – Methods, Materials, Models, Springer, Berlin, 2005, pp. 367–415.
[32] M. Masoud, P. Heitjans, Impedance Spectroscopy Study of Li Ion Dynamics in Single Crystal, Microcrystalline, Nanocrystalline, and Amorphous $LiNbO_3$, Defect and Diff. Forum 237-240 (2005) 1016–1021.
[33] P. Heitjans, M. Masoud, A. Feldhoff, M. Wilkening, NMR and Impedance Studies of Nanocrystalline and Amorphous Ion Conductors: Lithium Niobate as a Model System, Faraday Discuss. 134 (2007) 67–82.
[34] P. Fielitz, G. Borchardt, R.A. De Souza, M. Martin, M. Masoud, P. Heitjans, Oxygen-18 Surface Exchange and Diffusion in Li_2O-Deficient Single Crystalline Lithium Niobate, Solid State Sciences 10 (2008) 746–753.
[35] J. Rahn, E. Hüger, L. Dörrer, B. Ruprecht, P. Heitjans, H. Schmidt, Self-diffusion of Lithium in Amorphous Lithium Niobate Layers, Z. Phys. Chem. 226 (2012) 439–448.
[36] E. Hüger, J. Rahn, J. Stahn, T. Geue, P. Heitjans, H. Schmidt, Lithium Diffusion in Congruent $LiNbO_3$ Single Crystals at Low Temperatures Probed by Neutron Reflectometry, Phys. Chem. Chem. Phys. 16 (2014) 3670–3674.
[37] P. Rabiei, J. Ma, S. Khan, J. Chiles, S. Fathpour, Heterogeneous lithium niobate photonics on silicon substrates, Optics Express 21 (2013) 25573.
[38] P.O. Weigel, M. Savanier, C.T. DeRose, A.T. Pomerene, A.L. Starbuck, A.L. Lentine, V. Stenger, S. Mookherjea, Lightwave circuits in lithium niobate through hybride waveguides with silicon photonics., www.nature.com/articles/srep 22301, Science Reports 6 (2016), 22301.
[39] S. Indris, D. Bork, P. Heitjans, Nanocrystalline Oxide Ceramics Prepared by High-Energy Ball Milling, J. Mater. Synth. Process. 8 (2000) 245–250.
[40] P. Scherrer, Bestimmung der Größe und der inneren Struktur von Kolloidteilchen mittels Röntgenstrahlen, Göttinger Nachrichten 2 (1918) 98–100.
[41] G.K. Williamson, W.H. Hall, X-ray line broadening from filed aluminium and wolfram, Acta Met. 1 (1952) 22.
[42] D. Fink, Neutron Depth Profiling, HMI-B 539 (1996), ISSN 0936-0891.
[43] J.F. Ziegler, J.P. Biersack, The Stopping and Ranges of Ions in Matter, vol. 1, Pergamon, Oxford, 1985.

Biography

D. Fink Study at the Free University of Berlin (1974: PhD in Physics). Scientist at Hahn-Meitner-Institute Berlin (1974-2008). Since 2008: work at UAM Mexico as guest professor.